Alkali magmatism on a carbonaceous chondrite planetesimal

Jérôme Aléon[a,1], Alice Aléon-Toppani[b], Bernard Platevoet[c], Jacques-Marie Bardintzeff[c], Kevin D. McKeegan[d], and François Brisset[e]

[a]Institut de Minéralogie, de Physique des Matériaux et de Cosmochimie, UMR 7590, Sorbonne Université, Museum National d'Histoire Naturelle, CNRS, Université Pierre et Marie Curie, Institut de Recherche pour le Développement, 75005 Paris, France; [b]Université Paris-Saclay, CNRS, Institut d'Astrophysique Spatiale, 91405 Orsay, France; [c]Université Paris-Saclay, Sciences de la Terre, Volcanologie-Planétologie, UMR CNRS 8148 Geosciences Paris Sud, F-91405 Orsay, France; [d]Department of Earth, Planetary, and Space Sciences, University of California, Los Angeles, CA 90095-1567; and [e]Université Paris-Saclay, CNRS, Institut de Chimie Moléculaire et des Matériaux d'Orsay, 91405 Orsay Cedex, France

Edited by Mark H. Thiemens, University of California San Diego, La Jolla, CA, and approved February 26, 2020 (received for review November 7, 2019)

Recent isotopic and paleomagnetic data point to a possible connection between carbonaceous chondrites and differentiated planetary materials, suggesting the existence, perhaps ephemeral, of transitional objects with a layered structure whereby a metal-rich core is enclosed by a silicate mantle, which is itself overlain by a crust containing an outermost layer of primitive solar nebula materials. This idea has not received broad support, mostly because of a lack of samples in the meteoritic record that document incipient melting at the onset of planetary differentiation. Here, we report the discovery and the petrologic–isotopic characterization of UH154-11, a ferroan trachybasalt fragment enclosed in a Renazzo-type carbonaceous chondrite (CR). Its chemical and oxygen isotopic compositions are consistent with very-low-degree partial melting of a Vigarano-type carbonaceous chondrite (CV) from the oxidized subgroup at a depth where fluid-assisted metamorphism enhanced the Na content. Its microdoleritic texture indicates crystallization at an increasing cooling rate, such as would occur during magma ascent through a chondritic crust. This represents direct evidence of magmatic activity in a carbonaceous asteroid on the verge of differentiating and demonstrates that some primitive outer Solar System objects related to icy asteroids and comets underwent a phase of magmatic activity early in the Solar System. With its peculiar petrology, UH154-11 can be considered the long-sought first melt produced during partial differentiation of a carbonaceous chondritic planetary body, bridging a previously persistent gap in differentiation processes from icy cometary bodies to fully melted iron meteorites with isotopic affinities to carbonaceous chondrites.

alkali magmatism | early Solar System | planetary differentiation | O and Mg isotopes | meteorites

Planetary differentiation is the sum of processes by which planetesimals acquired a concentric layered structure akin to that of terrestrial planets with a metallic iron core overlain by a silicate mantle and crust. Meteorites provide a bona fide record of planetary formation processes and can be used to understand the differentiation processes. The early crystallization age (1, 2) of differentiated meteorites indicates that planetesimals which accreted during the first million years of the Solar System underwent complete core–mantle–crust differentiation, most likely upon heating by the decay of ^{26}Al. Later, accreted planetesimals remained undifferentiated chondrites with components out of chemical equilibrium with each other. Magmatism associated with differentiation was usually considered to be basaltic, as recorded by most achondrites, but the discovery of evolved achondrites with andesitic or trachyandesitic bulk chemistry has challenged this view (3–5). Siderophile element abundances even suggest that silicate melting may have taken place without formation of a metallic core (3). Further complication comes from paleomagnetic studies of carbonaceous chondrites (6–8) and magma ocean models (9, 10), which suggest that parent-bodies of the Vigarano-type carbonaceous chondrite (CV) and possibly Mighei-type carbonaceous chondrites (CM) may have been as large as 200 km in diameter (6–8) and may be partially differentiated with a metallic core and a chondritic crust (6–10). However, meteoritic samples that can clearly document the onset of silicate melting and constrain the beginning of planetary differentiation have so far been lacking. Here, we report the discovery and detailed characterization of an igneous clast found within a carbonaceous chondrite matrix and show how its petrogenesis sheds light on the onset of planetary differentiation and on the relationship between carbonaceous chondrites and differentiated asteroids.

Results and Discussion

Sample Description. UH154-11 is a bottle-shaped magmatic fragment, ~1.1 mm long by ~0.7 mm in its largest width, embedded in the Renazzo-type carbonaceous chondrite (CR) El Djouf 001. It has a very fine-grained doleritic texture similar to that observed in dykes on Earth (Fig. 1 and *SI Appendix*, Fig. S1) and is heavily fractured. It is dominantly composed of 1) elongated andesine plagioclase laths ($An_{40–50}$), 10 μm in width and up to ~100 μm in length, with length/width ratios averaging around 5; 2) approximately equant, sometimes skeletal, Fe-rich olivine ($Fo_{40–50}$) ~10 μm in size; and 3) augitic clinopyroxene ($Wo_{34–39}En_{29–41}Fs_{21–36}$) of variable shape, typically ~5 μm in size (Fig. 2 and *SI Appendix*, Table S1). Mineral intergrowths (Fig. 1) with 1) shards of clinopyroxene up to 20 μm long included within plagioclase; 2) skeletal-shape rims of plagioclase enclosing tiny clinopyroxene and olivine; and 3) inclusions of tiny clinopyroxene and minute melt inclusions in the outer rims of olivine are suggestive of a minimum-melt

Significance

In spite of magnetic and isotopic evidence revealing connections between the most primitive outer Solar System materials and differentiated bodies with a layered structure akin to terrestrial planets, the meteoritic record lacks samples that document the initiation of partial melting and the onset of planetary differentiation. Here, we describe a trachybasalt formed by very limited partial melting of a carbonaceous chondrite and crystallized as a dyke during ascent through the chondritic crust. This sample testifies of partial differentiation of outer Solar System carbonaceous planetesimals and can be considered as the long-sought first melt produced in differentiating small bodies.

Author contributions: J.A. and A.A.-T. designed research; J.A., A.A.-T., B.P., J.-M.B., K.D.M., and F.B. performed research; J.A., A.A.-T., B.P., J.-M.B., K.D.M., and F.B. analyzed data; and J.A., A.A.-T., B.P., J.-M.B., K.D.M., and F.B. wrote the paper.

The authors declare no competing interest.

This article is a PNAS Direct Submission.

[1]To whom correspondence may be addressed. Email: jerome.aleon@mnhn.fr.

This article contains supporting information online at https://www.pnas.org/lookup/suppl/doi:10.1073/pnas.1919550117/-/DCSupplemental.

First published March 30, 2020.

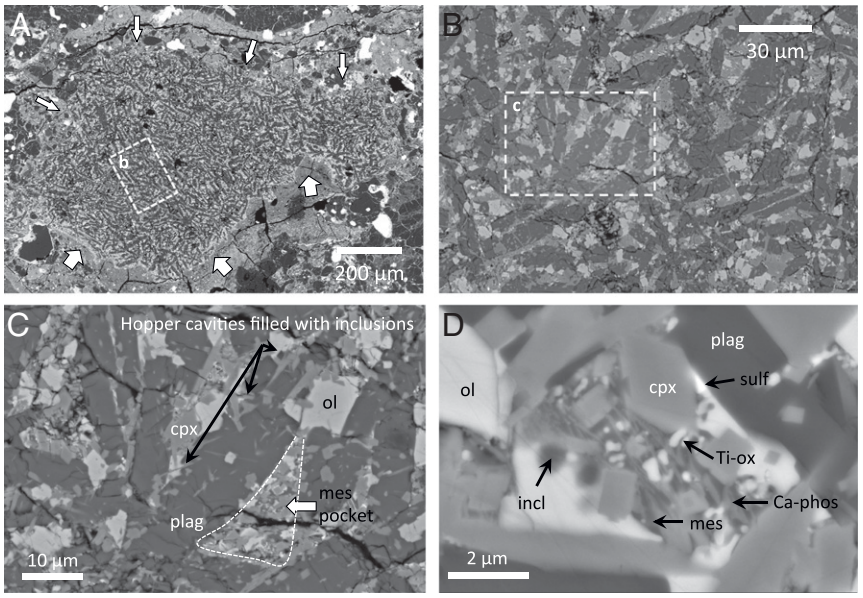

Fig. 1. Microphotographs of clast UH154-11. (*A*) Backscattered electron (BSE) image of the whole clast. Thin arrows, brecciated side; thick arrows, fine-grained rim around the altered side. (*B*) BSE image of typical texture. (*C*) BSE image illustrating crystal morphologies. Arrow, mesostasis pocket. (*D*) BSE image of a mesostasis pocket. Ca-phos, Ca-phosphate; cpx, clinopyroxene; incl, melt inclusion; mes, mesostasis; ol, olivine; plag, plagioclase; sulf, sulfide; Ti-ox, Ti-oxide.

assemblage with almost simultaneous crystallization of plagioclase, pyroxene, and olivine and a kinetically favored plagioclase growth. Abundant micrometer-sized pyroxene crystals of equant to needle shape and small olivine crystals are accumulated in residual pockets between the main plagioclase crystals (Fig. 1). These pockets also contained 100-nm-sized Ti-rich oxides with variable Fe content, dendritic submicrometer Ca-phosphates, and rare sulfide grains smaller than 100 nm, embedded in an interstitial glassy mesostasis appearing as patches too tiny for quantitative geochemical characterization (Fig. 1). Modal proportions yielded ∼45% plagioclase, ∼29% pyroxene, ∼12% olivine, and ∼15% of areas corresponding to mesostasis pockets, but also to fractures and holes in the thin section.

The crystal habits suggest dynamic crystallization at an increasing cooling rate, a feature characteristic of ascending magmas (*SI Appendix*, Fig. S1). This is notably the case for highly elongated plagioclase and its rim inclusions, indicating growth evolving toward a skeletal mode with trapping of tiny phases in crystal hopper cavities (11, 12). On Earth, this is commonly associated with fracturing during decompression, increase of supercooling, and change in crystallization mode (11, 12). The small amount of mesostasis indicates that when the melt finally quenched, the UH154-11 clast was largely crystallized (>>85%).

The bulk composition of UH154-11 is consistent with that of an Fe-rich trachybasalt having 5.8 wt% Na_2O and 15.1 wt% FeO_{tot} (Fig. 3 and *SI Appendix*, Table S2). Its calculated Cross, Iddings, Pirsson, and Washington (CIPW) composition includes normative nepheline, indicating that it is highly silica-undersaturated, and the differentiation index (13) indicating the degree of magmatic evolution is ∼39. This composition is relatively evolved, very alkaline, at the boundary between the trachybasalt and tephrite fields.

One side of the clast is brecciated and in direct contact with the host meteorite matrix and chondrule fragments without any evidence for interaction with the matrix (Fig. 1 and *SI Appendix*, Fig. S2). However, the other side is locally mantled by a fine-grained material analogous to the fine-grained rims around chondrules in carbonaceous chondrites (Fig. 1). This rim is enriched in Al and depleted in S, and Fe to some extent, compared to the regular El Djouf 001 matrix (*SI Appendix*, Fig. S3). A layer enriched in olivine and depleted in plagioclase delimits the contact between the clast and this fine-grained rim. Apart from this layer, no other obvious evidence of aqueous alteration or metamorphic modifications were found in the clast. The rim plus layer interface between the unaltered clast and the El Djouf 001 matrix suggests that UH154-11 underwent limited peripheral alteration and reacted with a first generation of matrix. The lack of interactions with matrix on the other side of the clast indicates that the observed brecciation in the CR parent-body occurred after alteration had ceased.

Precursor/Parent-Body. Oxygen (O) isotopic composition has long been used to identify genetically related meteorites. Despite its being trapped in a CR carbonaceous chondrite, the O isotopic

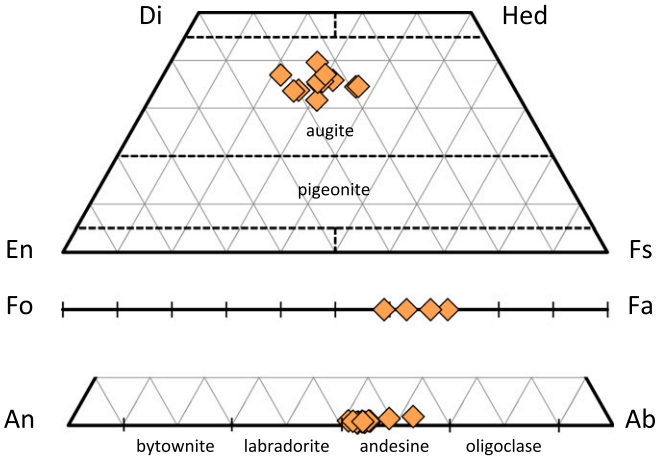

Fig. 2. Mineral chemistry of UH154-11 major minerals. (*Top*) Pyroxene composition. (*Middle*) Olivine composition. (*Bottom*) Plagioclase composition. Ab, albite; An, anorthite; Di, diopside; En, enstatite; Fa, fayalite; Fo, forsterite; Fs, ferrosilite; Hed, hedenbergite.

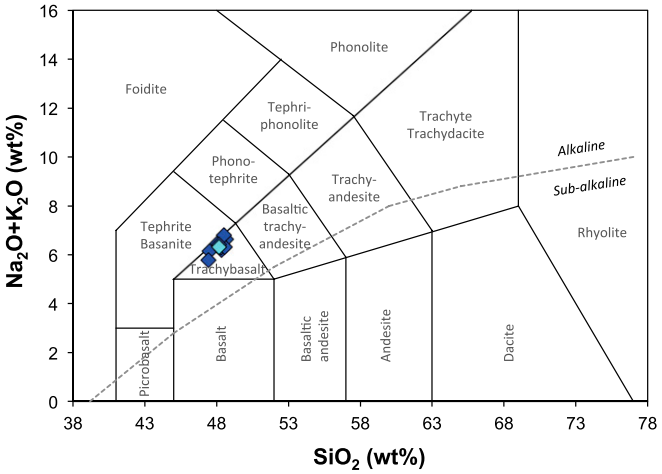

Fig. 3. Total alkali vs. silica classification diagram for clast UH154-11. Dark blue, individual rastered defocused analyses; light blue, average bulk composition. The dashed curve indicates the limit between the fields of alkaline and subalkaline magmas.

composition of UH154-11 is distinct from those of bulk CR chondrites, CR chondrule, and CR Ca, Al-rich inclusion (CAI) minerals. By contrast, it compares well with that of Vigarano- and Karoonda-type carbonaceous chondrites (CV–CK) and, most specifically, with the CV oxidized (CVox) subgroup (Fig. 4 and *SI Appendix*, Table S3). It is nearly identical to that of the Mokoia CVox chondrite and is within error of those from the Acfer 086 and Bali CV chondrites. It also matches the composition of CV chondrule mesostases and the most ^{16}O-poor minerals in CV CAIs. Because Na and K are both incompatible elements of similar geochemical behavior, they remain unfractionated to a first order during partial melting and can also be used to shed light on the source of the partial melt. The bulk Na/K ratio (wt%) of UH154-11 is about 17.5, much higher than in terrestrial basalts. Examination of 260 Na/K ratios from 157 chondrites representing 13 chondrite groups and a few ungrouped chondrites shows a typical chondritic value around 8.5 (*SI Appendix*). However, Ornans-type carbonaceous chondrites (CO), CVox, and CK chondrites have distinctly higher Na/K ratios (10.8, 11.1, and 11.9, respectively). Heterogeneous Na/K ratios with high Na/K ratios similar to that of the UH154-11 clast are observed in the CK chondrite Karoonda (up to 22.7) and CVox Grosnaja (up to 16.5). These chondrites are variably metamorphosed with evidence of Fe and Na redistribution during high-temperature fluid circulations (14), which could explain the high Na/K ratio of the magmatic source of UH154-11. Interestingly, metamorphosed CV chondrite clasts have a significant range of Na/K ratios, with more than half having Na/K ratios larger than or equal to that of UH154-11 and only two having subchondritic ratios (15). It is not clear if CK chondrites represent a metamorphosed equivalent of the CV chondrites originating from a deeper part of a common parent-body (16, 17) or if they come from different parent-bodies, as indicated by slightly different Cr isotope systematics (18) and by magnetite chemistries (19). In any case, the high Na/K ratio of UH154-11 is in line with derivation of the parent magma from a CV or CK chondritic source as implied by O isotopes and further suggests that this magma was produced by partial melting of chondritic material previously metamorphosed to some extent and enriched in Na by hydrothermal fluid circulations.

Partial Melting Conditions. The crystallization temperature can, in principle, be estimated from the Mg content in plagioclase (20), but this was analytically challenging given the small size of plagioclase laths and the ubiquitous embedded shards of clinopyroxene. Whether measured by electron microprobe or by nanoscale secondary ion mass spectrometry (NanoSIMS), temperatures deduced from MgO contents assuming a typical An_{40} plagioclase composition range between 1,000 °C and 1,400 °C. Further insights on the partial-melting conditions can be gained from comparison with laboratory experiments. Heating of the Allende CV chondrite at 1,200 °C yielded partial melts of basaltic composition for ∼20% melting (21). A better chemical match is found when comparing the bulk composition of UH154-11 with that of chondrite partial melts produced in experiments aiming at synthesizing evolved achondritic magmas (22, 23). The closest compositional match corresponds to temperatures in the 1,100 °C to 1,140 °C range and O fugacities near the iron–wustite (IW) buffer. Melt fractions in these experiments were estimated to be ∼15 to 20%. Still, the composition of UH154-11 is either enriched in Na relative to the higher-temperature experiments or depleted in SiO_2 relative to the lower-temperature experiments. This difference can be attributed to a significantly lower melt fraction. Alkali basalts or trachybasalts with a similar differentiation index on Earth are produced by decompression melting at very low melt fraction, lower than 10% for SiO_2 content near 45 to 48 wt% and often lower than 5% (24, 25). We therefore concluded that the partial melting temperature was likely near 1,100 °C and that the plagioclase crystallization temperature was close to that corresponding to the minimal MgO content, i.e., ∼1,015 °C. The melt fraction was well below 10% and most likely ≤5%. We determined the corresponding fO_2 using the bulk rock composition (26). Bulk Fe^{2+} and Fe^{3+} proportions were determined from the Fe^{2+} and Fe^{3+} content of pyroxene and olivine together with their modal proportions (assuming that the contribution of nano-sulfides and nano-oxides is negligible), for temperatures between 1,100 and 1,200 °C and pressures between 2 and 30 bars (as expected in small asteroidal bodies). The calculated fO_2 values were typically around

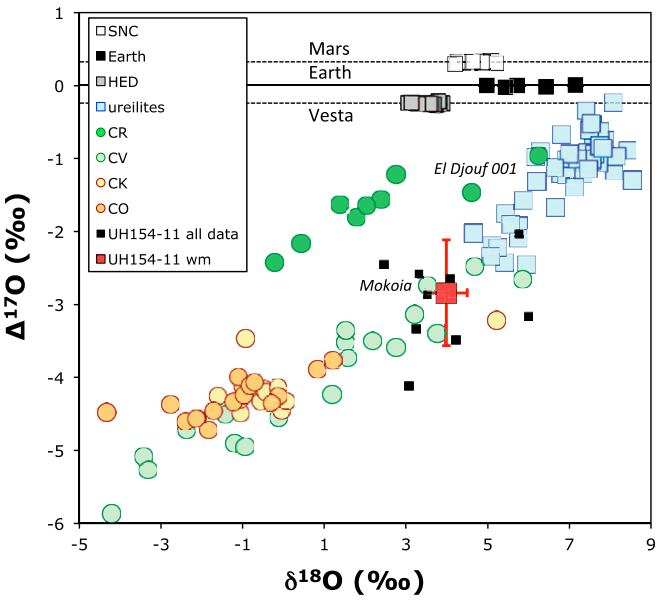

Fig. 4. O isotopic composition of clast UH154-11 compared with basaltic achondrites (squares) and carbonaceous chondrites (circles). Although not strictly basaltic, ultramafic ureilites are the achondrites closest in O isotopic composition to UH154-11. Errors on individual SIMS analyses have been omitted for clarity, and two standard errors are given for the weighted mean. HED, Howardites, Eucrites, Diogenites (meteorites from Vesta); SNC, Shergottites, Nakhlites, Chassignites (martian meteorites); wm, weighted mean. Data sources: carbonaceous chondrites (52), ureilites (53), HEDs (54), SNCs, and Earth (55).

IW-1.5 log units. Given the sources of uncertainties in the analyses of UH154-11 and the possibility that additional Fe^{3+} is hosted by nano-oxides, this estimate is certainly a lower limit. By contrast, the close chemical match with the partial melting experiments at the IW buffer (22, 23) suggests that the O fugacity is closer to the IW buffer. We therefore consider the latter to be a reasonable estimate. This fO_2 is consistent with that of a CV chondrite precursor, whereas CK chondrites are more oxidized (27).

Impact Melting or Magmatic Activity? A key issue is to determine whether UH154-11 results from impact melting or from magmatic activity deeper in a parent-body. As determined above, its chemical composition is in good agreement with partial melting of a chondritic source having an elevated Na/K ratio, with a very low melt fraction (<10%). This composition is different from the close-to-chondritic bulk composition of recognized impact melts from CV and CM chondrites (28) and expected from theoretical considerations, which favor large melting fractions upon impact (29). Possible chemical variations in impact melts are restricted to in situ small-scale melts, where only few minerals are melted, so that the melt composition depends directly on the contributing minerals (29). Compared to CV and CM impact melts, where large amounts of quenched glasses were identified (28), UH154-11 is highly crystallized. Furthermore, the texture of the crystal margins is consistent with an increasing cooling rate rather than the opposite (as expected in an impact). This increasing cooling rate is characteristic of magmas ascending in fractures and requires a strong thermal contrast between the magma at ∼1,100 °C and the surrounding host rock. Textures from dynamic crystallization experiments suggest a supercooling ΔT (thermal difference between effective crystallization and liquidus temperatures) of 60 to 100 °C, generated by a thermal contrast between the magma and the surrounding rocks (11, 12, 30, 31) possibly higher than 400 °C, as suggested by the textural similarity with a microgabbro comagmatic with a granitic magma (*SI Appendix*, Fig. S1). This would imply a surrounding body at ≤700 °C. By contrast, small-scale impact melts solidify nearly instantaneously and do not move or pool, due to the short duration of impact processes (29). We conclude that UH154-11 is an igneous rock resulting from very low partial melting of an oxidized chondritic precursor and subsequently transported from the source region to the final crystallization level by magmatic activity rather than by impact melting. The ∼400 °C thermal contrast and the almost entire crystallization (>>85%) indicate that the magma never reached the surface of the planetesimal.

Timing. Al/Mg dating of plagioclase shows an absence of ^{26}Mg excess attributable to ^{26}Al decay. The Mg isotopic data imply an upper limit on the initial $^{26}Al/^{27}Al$ ratio of 2.3×10^{-6}, which corresponds to an epoch of crystallization later than 3.3 million years (Ma) after CAI formation, assuming an initial Solar System ratio in CAIs of 5.23×10^{-5} (*SI Appendix*, Fig. S4 and Table S4). Having taken place after magmatic crystallization, the minimal secondary alteration undergone by UH154-11 can also provide a lower bound for the magmatic age. Given the preservation of mesostasis and ultra-fine-grained minerals in the clast interior, the alteration indicated by the reaction layer at the interface with the fine-grained rim on one side of UH154-11 was most likely a low-temperature process, consistent with aqueous alteration on the CR parent-body [<100 °C (32)] or on Bali-like oxidized CV chondrites [<300 °C (14, 33)]. Whether this minimal alteration occurred on the CV parent-body or in the CR parent-body is unclear. The comparison between the chemical compositions of the fine-grained rim, the clast, and the matrix of El Djouf 001 and of several CV chondrites (*SI Appendix*) suggests that the rim formed from a mixture of altered clast material and matrix (*SI Appendix*, Fig. S5). The best compositional matches are the Mokoia matrix, which only differs from the rim by addition of plagioclase and subtraction of sulfides, and the El Djouf 001 matrix, but in this case, leaching of Na and Ca in the rim is also required. This indicates that UH154-11 formed before or contemporaneously with low-temperature fluid circulations on these parent-bodies (*SI Appendix*, Fig. S6) estimated to have taken place about 3 to 4 Ma after CAIs in CV chondrites (33–35) and 4 to 5 Ma after CAIs in CR chondrites, with the exception of one very young age of 13 Ma after CAIs (32).

Implications for Planetary Differentiation. Nucleosynthetic isotopic anomalies (Cr, Ti, Mo, and W) revealed in the past few years suggest that meteorite parent-bodies define two broad families: those linked to carbonaceous chondrites and the noncarbonaceous meteorites including all other chondrite groups (36). Most differentiated meteorites belong to the noncarbonaceous family, but O, Cr, Mo, and W isotopes indicate that rare differentiated objects (including a peridotite) and several iron meteorite groups belong, instead, to the carbonaceous family (37, 38). This is key evidence that planetary differentiation affected not only noncarbonaceous objects, inferred to have formed in the inner Solar System, but also planetesimals grown from carbonaceous chondrites as well. This group includes the Eagle Station pallasite and ungrouped iron meteorites (39, 40) known to contain clasts with O isotopic compositions similar to that of CV, CO, and CK chondrites. Coupled Al/Mg and Hf/W dating of Eagle Station (41) indicates that metal–silicate segregation occurred late, between 5 and 10 Ma after CAIs, and thus argues for a protracted magmatic phase on some carbonaceous bodies compared to noncarbonaceous magmatic achondrites, such as eucrites or angrites, where core formation is believed to have occurred significantly earlier (1, 2). With a timing of formation similar to Eagle Station, UH154-11 is the first sample from a carbonaceous chondrite breccia that documents partial melting and magmatic activity on a carbonaceous chondrite planetesimal, which was most likely the CV chondrite planetesimal.

This magmatic activity implies that some portions of the interior of this planetesimal reached temperatures of at least the chondrite solidus. Several models (6–10) have considered chondritic planetesimals as keeping an undifferentiated crust, while at the same time having core temperatures above the chondrite liquidus resulting in a deep magma ocean and a convective molten metallic core. The specific conditions of formation of UH154-11, with a few percent partial melting at ∼1,100 °C, suggest a possible intermediate scenario in which the CV parent-body accreted too late to reach the chondrite liquidus upon heating by ^{26}Al decay, but still early enough to initiate alkali magmatism (Fig. 5). The 1,100 °C temperature exceeds the troilite–metal eutectic so that a sulfide-rich core produced by percolating Fe–Ni–S melts may have developed in this body (42). UH154-11 can be considered as the first melt produced from a chondrite, bridging the petrologic gap between primitive achondrites with evidence of centimeter-scale Fe–Ni–S migration (42, 43) and trachyandesitic achondrites crystallized from such a melt produced by low-degree partial melting of a chondrite (4, 5). Such a limited-melting scenario may account for the rarity of differentiated materials having isotopic affinities with CV chondrites (37) and differentiated clasts in CV chondrites. It can, however, be reconciled with paleomagnetic evidence if limited partial melts such as UH154-11 formed at the base of a shallow undifferentiated portion of a planetesimal having a differentiated interior and a deep magma ocean (Fig. 5). Together with the existence of iron meteorites and ungrouped achondrites having isotopic affinities with carbonaceous chondrites, this paleomagnetic evidence suggests the existence of an efficient sorting/segregation process yet to be identified to explain the dearth of differentiated materials related to CV chondrites.

According to thermal models (9), the CV parent-body must have accreted before about 1.5 Ma to have reached the solidus (where the solidus is assumed to be 1,200 °C; it may be slightly

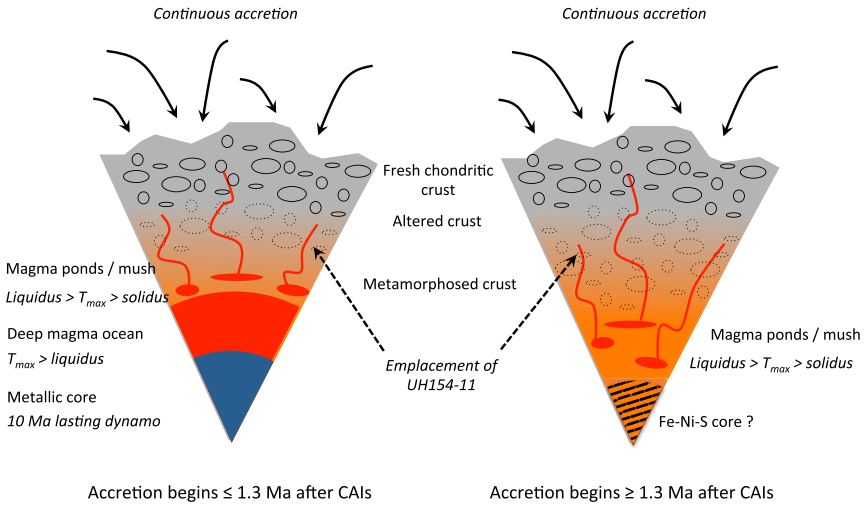

Fig. 5. Schematic of a CV-like parent-body internal structure about 4 Ma after CAI formation as deduced from the study of UH154-11. (*Left*) CV parent-body with a fully differentiated core formed by multistage or prolonged accretion. (*Right*) CV parent-body having undergone only incipient partial melting. The 1.3 Ma after CAIs is taken here as the latest possible start of accretion to achieve temperatures at depth between the chondritic solidus and liquidus (9). After 1.5 Ma, the maximal temperature does not reach the chondrite solidus (9).

later if 1,100 °C is considered). To reconcile this accretion age with radiometric ages of CV chondrules requiring accretion ∼3 Ma after CAIs (44), the CV parent planetesimal should have started to accrete before 1.5 Ma after CAI and continued accretion of undifferentiated materials during the next several million years (9). One could argue that prolonged accretion of the CV parent-body in a dynamically active protoplanetary disk may result in isotopically unrelated inner and outer portions of the parent-body. However, an efficient dynamical barrier between the inner and outer Solar System [for instance, the formation of Jupiter (38)] has been proposed to have operated in the first Ma of the Solar System. Such a barrier would imply that any body formed after 1 Ma in the carbonaceous chondrite region should be at least isotopically related with carbonaceous chondrites. This is probably the case of a CV parent-body formed by multistage or prolonged accretion.

The relationship between the magmatism at the origin of UH154-11 and the metasomatic alteration of CV chondrites remains unclear. On one hand, metasomatism of CV chondrites took place ∼4 Ma after CAIs (33–35), a timeframe consistent with formation of UH154-11 by partial melting of a chondritic source already similar to altered CVox chondrites and metamorphosed chondrite clasts enriched in Na. On the other hand, UH154-11 appears to have suffered some amount of alteration, suggesting that it could have formed before or contemporaneously with the alteration of CV or CR chondrites. As a consequence, emplacement of partial melts injected as sills and dykes in the undifferentiated crust of primitive chondritic planetesimals could be a potentially unrecognized source of heat and magmatic volatiles, such as alkalis, halogens, and water. These small intrusions could induce contact metamorphism at a local and heterogeneous scale and may also have contributed to Fe–alkali–halogen metasomatism. Extraction of UH154-11 requires subsequent kilometer-deep excavation of the CV planetesimal crust by a large impact (45), which could have contributed to the compaction of the rest of the CV chondrite parent-body (46, 47). Finally, trapping at the surface of the CR parent-body of a CV-derived clast confirms that clasts in chondrites could originate from different parent-bodies (48) and implies that CV and CR planetesimals probably formed in the same region of the protoplanetary disk, rather than being dynamically isolated from each other (49).

Along with other transitional objects, the magmatic history of UH154-11 indicates that many primitive asteroids have not always been static, frozen bodies. Rather, they once were dynamic objects having experienced fluid circulations, and sulfide and/or silicate magma migration processes affecting the host rock at various scales. UH154-11 points toward a continuum between fully undifferentiated and fully differentiated carbonaceous objects ranging from pristine chondritic/cometary bodies (porous anhydrous interplanetary dust particles), to hydrothermally altered chondrites/icy asteroids (Ivuna-type carbonaceous chondrites [CI], CM, and CR chondrites), metamorphosed chondrites (CO, CV, and CK chondrites), primitive achondrites (ungrouped), limited partial melts such as UH154-11 with more-or-less magmatic evolution, and, finally, fully differentiated objects (IIC, IID, IIF, IIIF, and IVAB iron meteorites). The existence of layered bodies, where increasing temperature resulted in complex structures of increasing petrologic types with depth or accretion age, suggests that future sample-return space missions from carbonaceous asteroids such as Hayabusa 2 and OSIRIS-REx may be confronted by a wide variety of geological materials.

Materials and Methods

The sample is a carbon-coated thin section of the Saharan CR chondrite El Djouf 001, loaned by A. N. Krot, University of Hawaii, Honolulu, HI (thin section UH154). UH154-11 was discovered during a survey of Ca, Al-rich objects in CR chondrites (50).

The mineralogical and petrographical characterization of UH154-11 was done by using scanning electron microscopes (SEMs) at Geosciences Paris Sud (GEOPS), Orsay, France, and University of California, Los Angeles (UCLA). Secondary electron and backscattered electron images were acquired at 15 keV. High-resolution images of mineral morphologies and energy-dispersive spectroscopic X-ray maps were acquired with field-emission gun SEMs at École Normale Supérieure (ENS) Geologie, Paris (with a 15-kV acceleration), and at the Institut de Chimie Moléculaire et des Matériaux d'Orsay, Orsay, France (with a 20-kV acceleration).

Mineral chemistry analyses were done at the CAMPARIS electron microprobe facility in Paris using a CAMECA SX100 electron probe. Individual analyses of olivine, plagioclase, and pyroxene were done in spot mode by using a 15-keV, 10-nA electron beam focused at 1 μm, with 20-s counting time for each element. Analyses were corrected by using classical Pochou and Pichoir (PAP) procedures. The bulk composition was determined in similar conditions by using a defocused beam scanned over 200-μm × 150-μm areas. Nine areas were analyzed from right to left with a 10-μm overlap between adjacent areas, covering the largest dimension of UH154-11. Electron microprobe mapping of sulfides and phosphorus were done separately

at the Microsonde Sud facility in Montpellier by using a 20-keV electron beam of 20 nA with a 0.1-s dwell time and a 2-μm step.

Modal abundances were determined by using ImageJ software by thresholding a high-resolution backscattered electron map at different gray levels corresponding to olivine (light gray), pyroxene (medium gray), plagioclase (dark gray), and holes/fractures/mesostasis (black and noisy areas). Masks of olivine, pyroxene, plagioclase, and black areas were calculated on a square 490-μm × 490-μm area covering most of the clast surface. A false color image was subsequently produced by recombination of olivine, plagioclase, pyroxene, and black masks in a red–green–blue–gray scheme (*SI Appendix*, Fig. S7).

O isotopes were measured with the CAMECA IMS 1270 ion probe at the UCLA, with methods similar to those of Aléon et al. (50). A 0.2-nA Cs^+ primary ion beam defocused in Kohler illumination mode was used to achieve ∼10- to 12-μm spots. Negative ^{16}O, ^{17}O, and ^{18}O secondary ions were acquired simultaneously by using the off-axis L1 Faraday cup and H1 electron multiplier for ^{16}O and ^{18}O, respectively, while ^{17}O was detected on the axial electron multiplier. Charge compensation was achieved by using carbon coating and a normal incidence electron flood gun. The vacuum was kept below 3×10^{-9} Torr using liquid N_2. The mass resolution at mass 17 was ∼6,000, enough to separate completely the ^{16}OH interference from ^{17}O. Ten measurements consisting of 15 cycles of 10 s were acquired after a 3-min presputtering to remove the C coating and reach the sputtering equilibrium. The instrumental mass fractionation was corrected by comparison to analyses of olivines from terrestrial mantle xenoliths (San Carlos olivine and 77-228 olivine) and from the Eagle Station pallasite and using Burma spinel. Matrix effects for mass fractionation in UH154-11 minerals relative to those standards could potentially reach several per mille due to variations in SiO_2 (pyroxene vs. olivine) and FeO content (magnesian vs. Fe-rich olivine). Because it was not possible to sample pure phases due to the complex mineralogy at the 10-μm scale, this effect was most likely responsible for the $\delta^{18}O$ dispersion of the analyses that sampled minerals in variable proportions. Examination of phase proportions within individual spots using high-resolution SEM images indeed showed that the two most ^{18}O-rich analyses are the most pyroxene-rich. Averaging multiple analyses decreases the contribution of the most fractionating phases. In addition, natural mass fractionation effects are very small at high temperature. As a result, the weighted mean of all analyses is expected to give a bulk O isotopic composition with a mass fractionation within ∼1‰ of the true bulk value and with an accurate ^{16}O excess reported as $\Delta^{17}O$ deviation relative to the terrestrial mass fractionation line. Excluding the pyroxene-rich analyses on the account of matrix effects would shift the bulk $\delta^{18}O$ and $\delta^{17}O$ values by −0.53‰ and −0.38‰, respectively, in even better agreement with CV chondrites. Uncertainties on individual analyses are 2 standard errors of the mean and include analytical precision and reproducibility on standards.

Mg isotopes were measured with the CAMECA NanoSIMS 50 at the Institut de Minéralogie, de Physique des Matériaux, et de Cosmochimie, Museum National d'Histoire Naturelle (MNHN) in Paris, by using a 26-pA O^- primary ion beam. Positive ^{23}Na, ^{24}Mg, ^{25}Mg, ^{26}Mg, and ^{27}Al secondary ions were detected simultaneously on five different electron multipliers by using a mass resolving power of around 10 000 (CAMECA definition), enough to separate all hydrides and doubly charged ion interferences. Analyses were done with a 3-μm raster of 256 × 256 pixels, using a blanking of 29% (corresponding to a 71% acquisition over 216 × 216 pixels) to avoid edge effects, with a dwell time of 1 ms/pixel and consisting of 50 cycles of 46 s each. A presputtering of 4 min was done with a 1-nA beam rastered over a 20-μm × 20-μm area to remove the C coating and achieve sputtering equilibrium. Plagioclase was targeted specifically for the Mg isotope and Al/Mg ratio analysis by imaging Na and Al within this presputtered area. The ^{26}Mg excesses in UH154-11 were determined relative to terrestrial standards by using the instrumental mass fractionation line calibrated with Vietnam spinel, San Carlos olivine, and T7 diopside using count rates similar to those during analysis of the clast, i.e., ∼5,000 counts per second of ^{24}Mg to avoid detector effects associated with large ion counts. Given the small range of Mg isotopic compositions on Earth, this line depends mainly on matrix effects for Mg isotopes, known to be strong in secondary ion mass spectrometry (SIMS) (51), and allows a better calibration of the mass fractionation, hence of the ^{26}Mg excesses due to the decay of ^{26}Al. The relative sensitivity factor for the Al/Mg ratio was determined by using Ni52 anorthite glass. Uncertainties are 2 standard errors of the mean and include analytical precision and reproducibility on standards. The upper limit on ^{26}Mg excess corresponds to 2 standard errors on the weighted mean of individual analyses.

Data Availability Statement. All data discussed in the paper are given in *SI Appendix*, Tables S1–S5.

ACKNOWLEDGMENTS. Staff of all the instruments used are thanked for help and maintenance, including G. Jarzebinsky (UCLA); D. Deldicque (ENS Paris); C. Merlet (Microsonde Sud); N. Rividi and M. Fialin (CAMPARIS); and S. Mostefaoui and A. Gonzalez-Cano (MNHN). V. Godard (GEOPS) prepared the terrestrial analogs sections. A. N. Krot provided the sample. This work was supported by the French Programme National de Planétologie of the CNRS-Institut National des Sciences de l'Univers and by the Actions Transversales du Museum program of the MNHN. The UCLA ion microprobe laboratory is partially supported by a grant from the NSF Instrumentation and Facilities Program. K.D.M. also was supported by the NASA Cosmochemistry Program.

1. M. Bizzarro, J. A. Baker, H. Haack, K. L. Lundgaard, Rapid timescales for accretion and melting of differentiated planetesimals inferred from ^{26}Al-^{26}Mg chronometry. *Astrophys. J.* **632**, L41–L44 (2005).
2. J. Baker, M. Bizzarro, N. Wittig, J. Connelly, H. Haack, Early planetesimal melting from an age of 4.5662 Gyr for differentiated meteorites. *Nature* **436**, 1127–1131 (2005).
3. J. M. D. Day *et al.*, Early formation of evolved asteroidal crust. *Nature* **457**, 179–182 (2009).
4. C. K. Shearer *et al.*, Non-basaltic asteroidal magmatism during the earliest stages of solar system evolution: A view from Antarctic achondrites Graves Nunatak 06128 and 06129. *Geochim. Cosmochim. Acta* **74**, 1172–1199 (2010).
5. A. Bischoff *et al.*, Trachyandesitic volcanism in the early Solar System. *Proc. Natl. Acad. Sci. U.S.A.* **111**, 12689–12692 (2014).
6. L. Carporzen *et al.*, Magnetic evidence for a partially differentiated carbonaceous chondrite parent body. *Proc. Natl. Acad. Sci. U.S.A.* **108**, 6386–6389 (2011).
7. J. Gattacceca, B. P. Weiss, M. Gounelle, New constraints on the magnetic history of the CV parent body and the solar nebula from the Kaba meteorite. *Earth Planet. Sci. Lett.* **455**, 166–175 (2016).
8. C. Cournède *et al.*, An early solar system magnetic field recorded in CM chondrites. *Earth Planet. Sci. Lett.* **410**, 62–74 (2015).
9. L. T. Elkins-Tanton, B. P. Weiss, M. T. Zuber, Chondrites as samples of differentiated planetesimals. *Earth Planet. Sci. Lett.* **305**, 1–10 (2011).
10. S. Sahijpal, G. Gupta, Did the carbonaceous chondrites evolve in the crustal regions of partially differentiated asteroids? *J. Geophys. Res.* **116**, E06004 (2011).
11. G. E. Lofgren, "Experimental studies on the dynamic crystallization of silicate melts" in *Physics of Magmatic Processes*, R. B. Hargraves, Ed. (Princeton University Press, Princeton, NJ, 1980), pp. 487–543.
12. B. Welsch, F. Faure, V. Famin, A. Baronnet, P. Bachelery, Dendritic crystallization: A single process for all the textures of olivine in basalts? *J. Petrol.* **54**, 539–574 (2013).
13. C. P. Thornton, O. F. Tuttle, Chemistry of igneous rocks. 1: The differentiation index. *Am. J. Sci.* **258**, 664–684 (1960).
14. A. N. Krot *et al.*, Progressive alteration in CV3 chondrites: More evidence for asteroidal alteration. *Meteorit. Planet. Sci.* **33**, 1065–1085 (1998).
15. K. Jogo, K. Nagashima, I. D. Hutcheon, A. N. Krot, T. Nakamura, Heavily metamorphosed clasts from the CV chondrite breccias Mokoia and Yamato-86009. *Meteorit. Planet. Sci.* **47**, 2251–2268 (2012).
16. R. C. Greenwood, I. A. Franchi, A. T. Kearsley, O. Alard, The relationship between the CK and CV chondrites. *Geochim. Cosmochim. Acta* **74**, 1684–1705 (2010).
17. J. T. Wasson, J. Isa, A. E. Rubin, Compositional and petrographic similarities of the CV and CK chondrites: A single group with variations in textures and volatiles concentrations attributed to impact heating, crushing, and oxidation. *Geochim. Cosmochim. Acta* **108**, 45–62 (2013).
18. Q.-Z. Yin, M. E. Sanborn, K. Zeigler, "Testing the common source hypothesis for CV and CK chondrites parent body using $\Delta^{17}O$-$\varepsilon^{54}Cr$ isotope systematics" in *48th Lunar and Planetary Science Conference* (Lunar and Planetary Institute, Houston, TX, 2017), abstr. 1771.
19. T. L. Dunn, J. Gross, M. A. Ivanova, S. E. Runyon, A. M. Bruck, Magnetite in the unequilibrated CK chondrites: Implications for metamorphism and new insights into the relationship between the CV and CK chondrites. *Meteorit. Planet. Sci.* **51**, 1701–1720 (2016).
20. J. Longhi, D. Walker, J. F. Hays, Fe and Mg in plagioclase. *Proc. Lunar Planet. Sci. Conf.* **7**, 1281–1300 (1976).
21. A. J. G. Jurewicz, D. W. Mittlefehldt, J. H. Jones, Experimental partial melting of the Allende (CV) and Murchison (CM) chondrites and the origin of asteroidal basalt. *Geochim. Cosmochim. Acta* **57**, 2123–2139 (1993).
22. T. Usui, J. H. Jones, D. W. A. Mittlefehldt, Partial melting study of an ordinary (H) chondrite composition with application to the unique achondrite Graves Nunataks 06128 and 06129. *Meteorit. Planet. Sci.* **50**, 759–781 (2015).
23. N. G. Lunning *et al.*, Partial melting of oxidized planetesimals: An experimental study to test the formation of oligoclase-rich achondrites Graves Nunataks 06128 and 06129. *Geochim. Cosmochim. Acta* **214**, 73–85 (2017).
24. D. P. McKenzie, The generation and compaction of partially molten rocks. *J. Petrol.* **25**, 713–765 (1984).
25. M. Caroff, R. C. Maury, G. Guille, J. Cotton, Partial melting below Tubuai (Austral Islands, French Polynesia). *Contrib. Mineral. Petrol.* **127**, 369–382 (1997).

26. K. D. Jayasuriya, H. St. C. O'Neill, A. J. Berry, S. J. Campbell, A Mössbauer study of the oxidation state of Fe in silicate melts. *Am. Mineral.* **89**, 1597–1609 (2004).
27. K. Righter, K. E. Neff, Temperature and oxygen fugacity constraints on CK and R chondrites and implications for water and oxidation in the early solar system. *Polar Sci.* **1**, 25–44 (2007).
28. N. G. Lunning *et al*., CV and CM chondrite impact melts. *Geochim. Cosmochim. Acta* **189**, 338–358 (2016).
29. K. Keil, D. Stoeffler, S. G. Love, E. R. D. Scott, Constraints on the role of impact heating and melting in asteroids. *Meteoritics* **32**, 349–363 (1997).
30. G. E. Lofgren, An experimental study of plagioclase crystal morphology: Isothermal crystallization. *Am. J. Sci.* **274**, 243–273 (1974).
31. S. E. Swanson, Relation of nucleation and crystal-growth rate to the development of granitic textures. *Am. Mineral.* **62**, 966–978 (1977).
32. C. E. Jilly-Rehak, G. R. Huss, K. Nagashima, ^{53}Mn-^{53}Cr radiometric dating of secondary carbonates in CR chondrites: Timescales for parent body alteration. *Geochim. Cosmochim. Acta* **201**, 224–244 (2017).
33. K. Jogo *et al*., Mn-Cr ages and formation conditions of fayalite in CV3 carbonaceous chondrites: Constraints on the accretion ages of chondritic asteroids. *Geochim. Cosmochim. Acta* **199**, 58–74 (2017).
34. P. M. Doyle *et al*., Early aqueous activity on the ordinary and carbonaceous chondrite parent bodies recorded by fayalite. *Nat. Commun.* **6**, 7444 (2015).
35. G. J. MacPherson, K. Nagashima, A. N. Krot, P. M. Doyle, M. A. Ivanova, ^{53}Mn-^{53}Cr chronology of Ca-Fe silicates in CV3 chondrites. *Geochim. Cosmochim. Acta* **201**, 260–274 (2017).
36. P. H. Warren, Stable-isotopic anomalies and the accretionary assemblage of the Earth and Mars: A subordinate role for carbonaceous chondrites. *Earth Planet. Sci. Lett.* **311**, 93–100 (2011).
37. M. E. Sanborn, Q.-Z. Yin, A. J. Irving, T. E. Bunch, "Differentiated planetesimals with chondritic crusts: New Δ^{17}O-ε^{54}Cr evidence in unique, ungrouped achondrites for partial melting of the CV/CK and CO parent bodies" in *46th Lunar and Planetary Science Conference* (Lunar and Planetary Institute, Houston, TX, 2015), abstr. 2259.
38. T. S. Kruijer, C. Burkhardt, G. Budde, T. Kleine, Age of Jupiter inferred from the distinct genetics and formation times of meteorites. *Proc. Natl. Acad. Sci. U.S.A.* **114**, 6712–6716 (2017).
39. E. J. Olsen *et al*., Mbosi: An anomalous iron with unique silicate inclusions. *Meteorit. Planet. Sci.* **31**, 633–639 (1996).
40. D. J. Malvin, J. T. Wasson, R. N. Clayton, T. K. Mayeda, W. da Silva Curvello, Bocaiuva—A silicate-inclusion bearing iron meteorite related to the Eagle-Station pallasites. *Meteoritics* **20**, 259–273 (1985).
41. T.-H. Luu, M. Chaussidon, J.-L. Birck, Timing of metal–silicate differentiation in the Eagle Station pallasite parent body. *C. R. Geosci.* **346**, 75–81 (2014).
42. T. J. McCoy *et al*., A petrologic, chemical, and isotopic study of Monument Draw and comparison with other acapulcoites: Evidence for formation by incipient partial melting. *Geochim. Cosmochim. Acta* **60**, 2681–2708 (1996).
43. T. J. McCoy *et al*., Graves Nunataks 95209: A snapshot of metal segregation and core formation. *Geochim. Cosmochim. Acta* **70**, 516–531 (2006).
44. K. Nagashima, A. N. Krot, M. Komatsu, ^{26}Al–^{26}Mg systematics in chondrules from Kaba and Yamato 980145 CV3 carbonaceous chondrites. *Geochim. Cosmochim. Acta* **201**, 303–319 (2017).
45. T. M. Davison, D. P. O'Brien, F. J. Ciesla, G. S. Collins, The early impact histories of meteorite parent bodies. *Meteorit. Planet. Sci.* **48**, 1894–1918 (2013).
46. P. A. Bland *et al*., Pressure-temperature evolution of primordial solar system solids during impact-induced compaction. *Nat. Commun.* **5**, 5451 (2014).
47. A. W. Tait, K. R. Fisher, P. Srinivasan, J. I. Simon, Evidence for impact induced pressure gradients on Allende CV3 parent body: Consequences for fluid and volatile transport. *Earth Planet. Sci. Lett.* **454**, 213–224 (2016).
48. J. Gattacceca *et al*., Young asteroid mixing revealed in ordinary chondrites: The case of NWA 5764, a polymict LL breccia with L clasts. *Meteorit. Planet. Sci.* **52**, 2289–2304 (2017).
49. E. M. M. E. Van Kooten *et al*., Isotopic evidence for primordial molecular cloud material in metal-rich carbonaceous chondrites. *Proc. Natl. Acad. Sci. U.S.A.* **113**, 2011–2016 (2016).
50. J. Aléon, A. N. Krot, K. D. McKeegan, Calcium-aluminum-rich inclusions and amoeboid olivine aggregates from the CR carbonaceous chondrites. *Meteorit. Planet. Sci.* **37**, 1729–1755 (2002).
51. T.-H. Luu *et al*., High precision Mg isotope measurements of meteoritic samples by secondary ion mass spectrometry. *J. Anal. At. Spectrom.* **28**, 67–76 (2013).
52. R. N. Clayton, T. K. Mayeda, Oxygen isotope studies of carbonaceous chondrites. *Geochim. Cosmochim. Acta* **63**, 2089–2104 (1999).
53. R. N. Clayton, T. K. Mayeda, Oxygen isotope studies of achondrites. *Geochim. Cosmochim. Acta* **60**, 1999–2017 (1996).
54. R. C. Greenwood, I. A. Franchi, A. Jambon, P. C. Buchanan, Widespread magma oceans on asteroidal bodies in the early Solar System. *Nature* **435**, 916–918 (2005).
55. I. A. Franchi, I. P. Wright, A. S. Sexton, C. T. Pillinger, The oxygen-isotopic composition of Earth and Mars. *Meteorit. Planet. Sci.* **34**, 657–661 (1999).